

DOI: 10.1002/adfm.200500284

Energy Collection, Transport, and Trapping by a Supramolecular Organization of Dyes in Hexagonal Zeolite Nanocrystals**

By Claudia Minkowski, Robert Pansu, Minako Takano, and Gion Calzaferri*

The incorporation of guest molecules into the cavities of molecular sieves leads to a large variety of highly interesting materials. Zeolite L—an aluminosilicate with one-dimensional channels of open diameter 7.1 Å—is a very versatile material for building highly organized host–guest systems. We present materials where organic dye molecules have been incorporated into the channels of zeolite L by means of diffusion, to build artificial photonic antenna systems. The channel entrance can be plugged by adding closure molecules that then connect the guest molecules inside with materials or molecules outside of the zeolite channels, since they can act as extensions of the interior of the zeolite crystal. The photophysical processes taking place in such dye-loaded zeolite L antennae can be studied either on single-micrometer- or submicrometer-sized crystals or on crystals dispersed in a solvent or coated as thin layers on a support. The energy-transfer process occurring is of the Förster-type, and its transfer rate can be tuned by separating the donor dyes and the acceptor dyes locally by varying amounts of spacer molecules. The distribution of the dye molecules and empty sites within a zeolite crystal has been modeled by means of a Monte Carlo simulation. The Förster energy migration and transfer steps are described as a random walk.

1. Introduction

Plant photosynthesis, the conversion of light into chemical energy, is endlessly fascinating. Just as a radio uses an antenna to absorb electromagnetic waves from the atmosphere, plants use their chlorophyll to capture certain wavelengths of visible light and pass its energy on to their photosynthetic apparatus.^[1,2] Such “photonic antennae” would also be of great value for technical applications, particularly for a new, more highly efficient generation of solar cells. Several interesting attempts are presented in the literature, for example, panchromatic chromophore mixtures in an AlPO₅ molecular sieve, faujasite-incorporated dye molecules, or polymer-embedded iridium complexes that show interesting luminescence properties.^[3–6] Promising results were attained with artificial photonic antennae, where a green fluorescent dye was introduced into the linear channels of zeolite crystals in order to capture light. When the fluorescent dye is irradiated, a small portion of the energy released is dispersed as vibrations throughout the molecules; the rest of the energy is emitted as fluorescence. When the dye molecules are immobilized in channels that traverse the crystals parallel to their long axes, they are neatly packed adjacent

to each other. This allows them to transfer the excitation energy directly—without conversion into light—from molecule to molecule. The special feature of these structures is this: the openings of the channels are plugged with a second type of fluorescent dye, a so-called stopcock molecule.^[7] The two types of molecules are precisely tuned to each other; the stopcocks are thus also able to accept excitation energy from the dyes inside the channel, but they are not able to pass it back. The stopcocks re-emit the energy as fluorescence on the surface of the crystals, or, in a more advanced setup, transfer it without radiation to a photoelectronic or a photochemical device. This “receiving” antenna can alternatively be made into a “transmitter” if the two fluorescent dyes are switched; the stopcocks then capture energy from outside, which they pass on to the molecules inside the crystals. These then fluoresce, which is useful for making, for example, light-emitting diodes.^[8,9] Herein, we present different types of dye-loaded zeolite L antenna materials—depending on the stage of organization of the dye molecules—and their applications. This reveals the importance of the stopcock molecules that act as a connection between the molecules inside the channels and materials or molecules outside the crystal. Furthermore, we focus experimentally and theoretically on the behavior of the electronic-excitation energy transfer among dye molecules within highly ordered zeolite materials, when the donors and the acceptors are locally separated by a certain number of spacer molecules.

[*] Prof. G. Calzaferri, C. Minkowski
Department of Chemistry and Biochemistry, University of Bern
CH-3012 Bern (Switzerland)
E-mail: gion.calzaferri@iac.unibe.ch

Dr. R. Pansu, M. Takano
PPSM, École Normale Supérieure de Cachan
F-94235 Cachan Cedex (France)

[**] This work was supported by the Schweizerischer Nationalfonds zur Förderung der wissenschaftlichen Forschung, projects NRP-47 4047-57481 and NF 200020-105140/1. The time-resolved data reported in Table 2 were measured by Katsiaryna Lutkouskaya.

2. Materials

2.1. Host Material and Dyes

Zeolites are porous silicates of different size, shape, and geometry that can encapsulate a large variety of guest molecules.

Promising results were obtained with colloidal zeolites where mesoporous spheres are used as a template to prepare zeolite monoliths.^[10,11] Zeolite L is a crystalline aluminosilicate with hexagonal symmetry.^[12,13] Its anionic framework and the positions of the charge-compensating cations are illustrated in Figures 1a–d. The crystals consist of cancrinite cages (ϵ -cages) linked by double six-membered rings. These units form columns in the c direction that are connected, and thus form a twelve-membered ring with a free diameter of 0.71 nm. This gives rise to one-dimensional channels running through the whole crystal, with a largest free diameter of 1.26 nm and a unit-cell length of 0.75 nm. The main channels are linked via non-planar eight-membered rings which form an additional two-dimensional channel system with ring opening of about 0.15 nm. The center-to-center distance between two main channels is 1.84 nm. The hexagonal structure of the zeolite L material is visible in the scanning electron microscopy image shown in Figure 1e. This also illustrates that the shape of the crystals can be described well by assuming cylindrical morphology.^[14] The number of channels lying parallel to the c axis is equal to $0.265(d_c)^2$, where d_c is the diameter of the cylinder in nanometers. As an example, a crystal with a 550 nm diameter consists of about 8×10^4 parallel channels.

Zeolite L has an anionic framework. Four different cation sites (A, B, C, D) have been reported. A is in the center of the double six-membered ring, B is in the center of the ϵ -cage, C lies midway between the centers of two adjacent ϵ cavities, and D is inside the main channel near the wall of the eight-membered ring. Dehydrated zeolite L shows an additional cation site located between two adjacent A sites and is indicated by E in Figure 1c. The water molecules in the large cavities of zeolite L have been reported to behave like an intercrystalline liquid, whereas they seem to build clusters around the cations in the smaller pores.^[15] The stoichiometry of zeolite L with mono-

valent cations M^+ is $(M)_9[Al_9Si_{27}O_{72}] \cdot nH_2O$, where n equals 21 in fully hydrated materials, and 16 at about 22 % relative humidity. We have synthesized zeolite L crystals in the size range of 30 to approximately 7000 nm.^[16]

Scheme 1 shows some of the dye molecules that have been incorporated into the channels of zeolite L.

2.2. Dye-Loaded Zeolite L Materials

The incorporation of guest molecules into the cavities of molecular sieves leads to a large variety of highly interesting materials.^[17] We now present materials where molecules—shown in Scheme 1—are incorporated into the channels of zeolite L.^[8,18,19] The cationic dyes can be incorporated into the channels via ion exchange; the neutral dyes are inserted from the gas phase. Materials that have been synthesized by us to date can be divided into four categories, depending on the stage of organization of the dye molecules, as seen in Figure 2.

Single-dye materials contain zeolite L crystals that are filled with only one kind of dye molecule. Interesting photophysical properties of the dye molecules can be studied, for example, polarization experiments (since the host lattice implies a strict arrangement of the guest molecule),^[20] light-induced reorganization such as photoisomerization,^[21] or changes in the conformation of the guest molecules due to steric constraints imposed by the zeolite.^[22] Furthermore, such crystals can act as nanolasers, see Figure 2a bottom, where the dye molecules start to lase by increasing the excitation power.^[23]

Mixed-dye materials consist of zeolite L crystals randomly filled with different dye molecules. This can be realized when the dyes enter the channels at about the same speed. If the spectral properties of the dyes are such that the emission spectra of one dye (donor) has a large overlap integral with the ex-

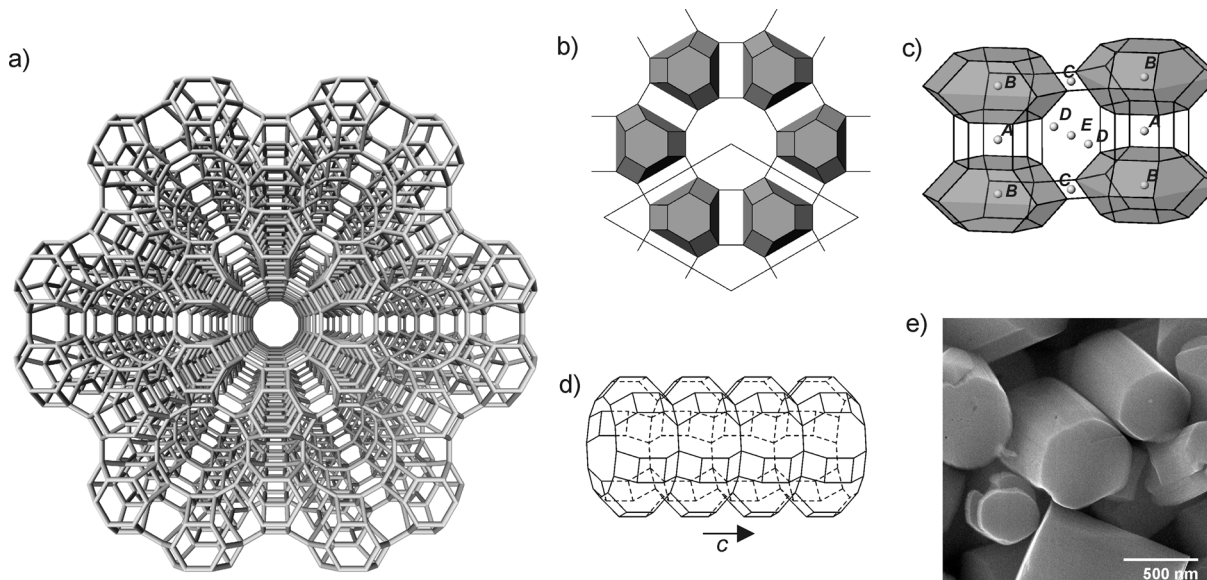
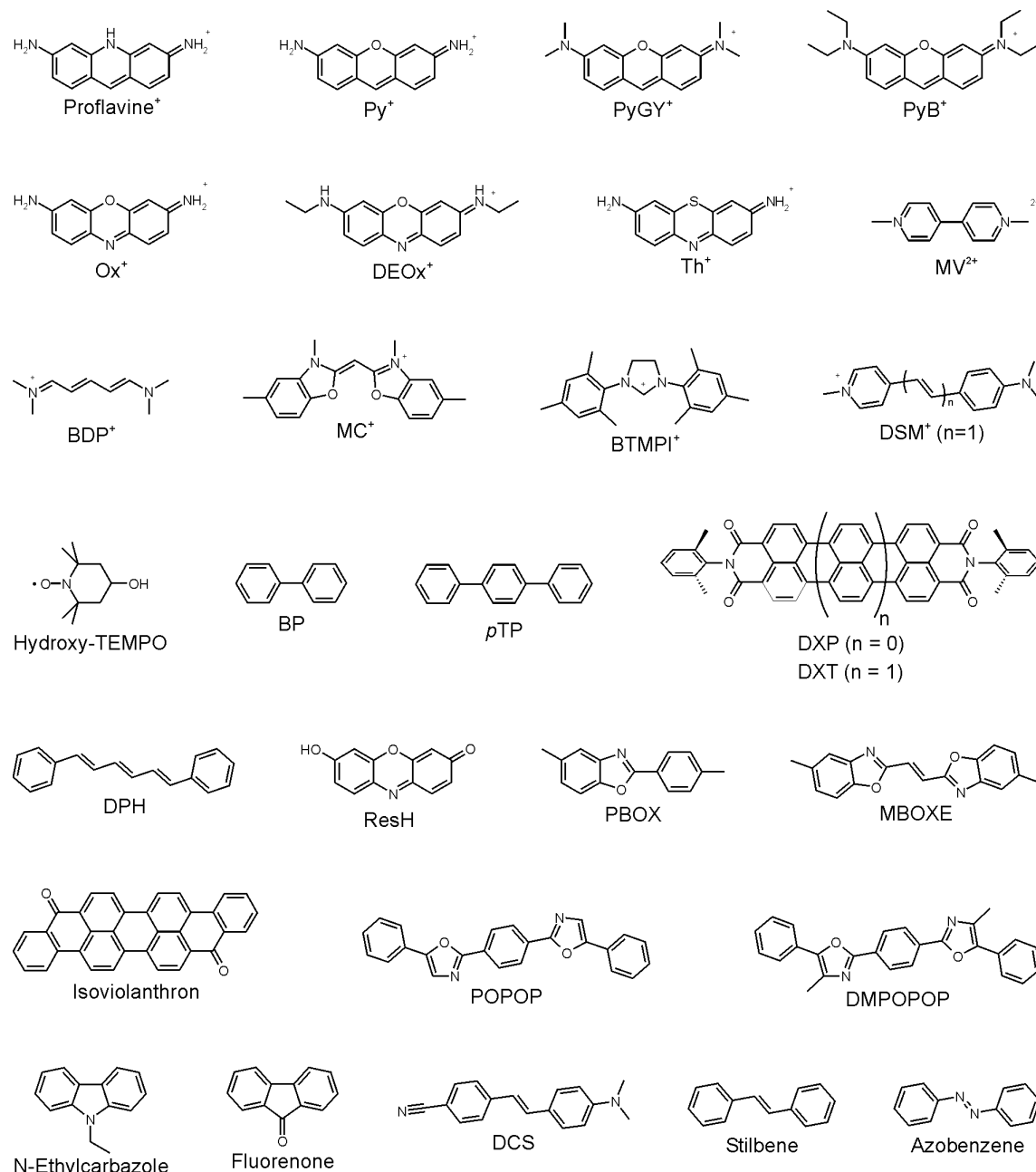


Figure 1. Zeolite L framework: a) projection along the c axis, b) with the cancrinite cages highlighted as polyhedra, c) section showing the different cationic positions A to E, d) side view of the 12-ring channel, e) scanning electron microscopy image of zeolite L crystals.



Scheme 1. Examples of dyes that have been incorporated in the channels of zeolite L.

citation spectra of the other dye (acceptor), Förster-type energy transfer from one dye to the other can be observed. A visual demonstration of the energy transfer is based on the observation that pyronine (Py⁺) and oxonine (Ox⁺) are inserted into zeolite L at about equal rates. It is therefore possible to control the mean distance between donors and acceptors by varying the concentration. Electronically excited donors transfer their energy to the acceptors at a rate that depends on their separation.^[24] The bottom image in Figure 2b shows 7 luminescent samples of zeolite L crystals filled with different amounts of Py⁺ (donor) and Ox⁺ (acceptor). Owing to their favorable spectral properties and their high fluorescence quantum yields, this

donor–acceptor pair exhibits remarkable excitation-energy-transport capability via Py⁺ energy carriers to luminescent Ox⁺ traps. In all cases, Py⁺ was selectively excited at 485 ± 5 nm, where the absorption of Py⁺ is strong and that of Ox⁺ very weak. The reference materials, samples 1 and 7, are loaded with only Py⁺ and Ox⁺, respectively. As can be seen, only the Py⁺–zeolite L sample 1 is excited. The other samples contain a 1:1 mixture of Py⁺ and Ox⁺ with increasing concentrations. We observe in sample 2 mainly the green luminescence of Py⁺. This means that the energy transfer is unimportant. However, the yellow color of sample 3 is due to a mixture of green and red luminescence, which means that energy transfer is signifi-

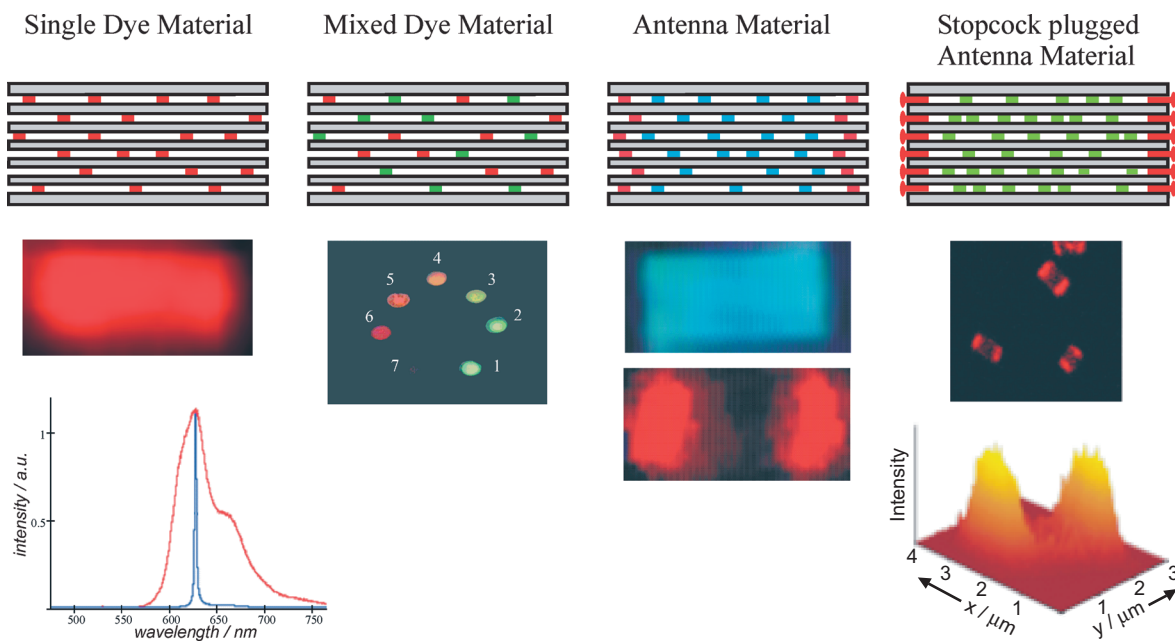


Figure 2. Overview of dye–zeolite L materials. *Single-dye material.* Top: Zeolite L crystal loaded with one kind of dye molecule. Middle: Fluorescence microscopy image of a zeolite L crystal containing red-light emitting dyes. Bottom: Fluorescence (red) of an Ox^+ -loaded zeolite L crystal after electronic excitation. By increasing the excitation power, the crystal starts to laze, as illustrated by the narrow emission band with a full width at half maximum (FWHM) of 2 nm (blue); the crystal has a length of about 1000 nm. *Mixed-dye material.* Top: Zeolite L crystal randomly mixed loaded with two different kinds of dye molecules. Bottom: Photograph of the fluorescence of dye-loaded zeolite L layers upon monochromatic irradiation at 485 ± 5 nm and observation through a cut-off filter. Probes 1 and 7 are references loaded with Py^+ and Ox^+ , respectively. Probes 2 to 6 contain a 1:1 mixture of Py^+ and Ox^+ with increasing concentration from 2 to 6. *Antenna material.* Top: Zeolite L crystal consecutively loaded with different dye molecules. Bottom: Fluorescence microscopy image of such a zeolite L crystal, containing blue-light-emitting dyes in the middle (middle) and red-light-emitting dyes at the channels endings (bottom). *Stopcock-plugged antenna material.* Top: Zeolite L crystal loaded with one kind of dye molecule and then sealed with a stopcock molecule. Middle: Confocal microscopy image of the red-light emission of the stopcock molecules located at the channel endings. Bottom: Confocal microscopy image of the local fluorescence intensity of a crystal with fluorescing stopcocks at the channel endings.

cant in this sample. It becomes more and more important with increasing concentration, so that from sample 5 on, the red luminescence stemming from Ox^+ is dominant.

For the *antenna materials*, the dyes are incorporated consecutively into the channels of zeolite L. Since the conditions are such that the dyes cannot glide past each other, the crystal is then divided into compartments where the density of one dye is dominant. If first a donor is incorporated and then an acceptor, the energy after selective excitation of the donor is transported from the middle to the channel endings, or vice versa if an acceptor is incorporated first. According to this transfer process, crystals also containing three different dyes can be synthesized.^[25]

For the *stopcock-plugged antenna materials*, as the name suggests, the channels are blocked with “plugs”—the so-called stopcock molecules.

2.3. The Stopcock Principle

Stopcock molecules have a narrow label, which can penetrate into the channels of zeolite L, and a head that is too large to be inserted, resembling a champagne cork (see Fig. 3). The label and head are connected by an inert, flexible spacer. Owing to this shape, they are able to plug the channel entrances.

These stopcock molecules connect the guest molecules inside with materials or molecules outside the zeolite channels, since they act as extensions of the interior of the zeolite crystal.^[26] The stopcocks can be reaction centers of: i) molecular dimensions, for example, a head of a stopcock molecule, which changes its properties as a function of pH, or the presence of a specific molecule; ii) macromolecular dimensions, such as photoinducing or conducting polymers, quantum dots, or semiconductors; and iii) macroscopic dimensions, such as semiconductors, conductors, and quantum wells. Furthermore, they can prevent small molecules, such as H_2O or O_2 , from diffusing into the channels.^[8]

Communication via energy transfer can be achieved by using stopcocks containing a strongly fluorescing unit. Such stopcock molecules can either trap the electronic excitation energy (acceptor stopcock) from a donor inside the channels or inject electronic excitation energy to an acceptor inside the channels (donor stopcock). We distinguish between different types of stopcock molecules, depending on the way they are linked to the channel entrances. *Reversible stopcocks* are only weakly bound to the zeolite framework.^[7,27] They are attached by adsorption. An example is the green fluorescing B493/503 molecule that can inject its excitation energy to the red-light emitting Ox^+ molecules inside the zeolite, see Figure 4 top, left. Figure 4 top, right shows the emission spectra of 30 nm long

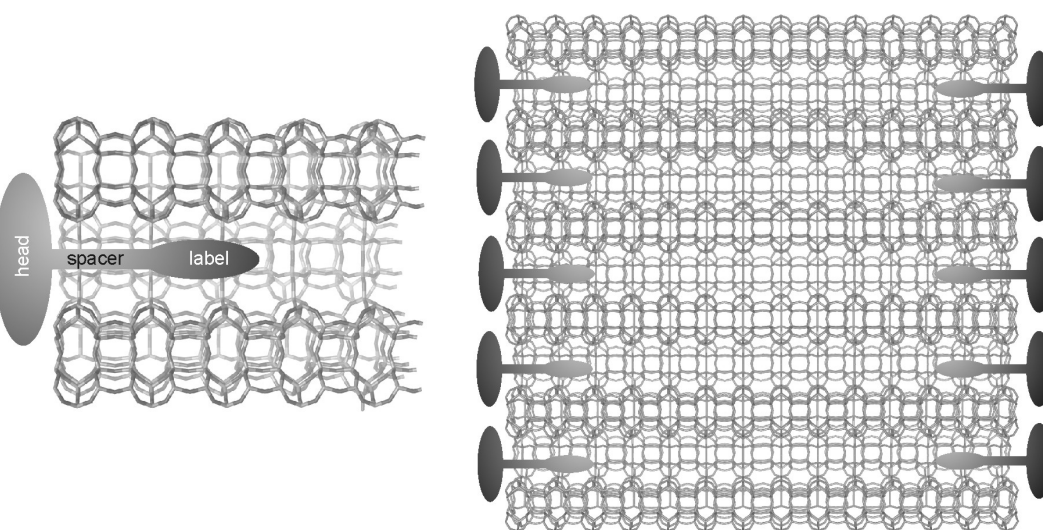


Figure 3. Stopcock principle. Left: Typical shape of a stopcock with a label that penetrates the channel and a head that is too large to enter. Label and head are connected with an inert flexible spacer. Right: A few channels that are plugged with stopcocks.

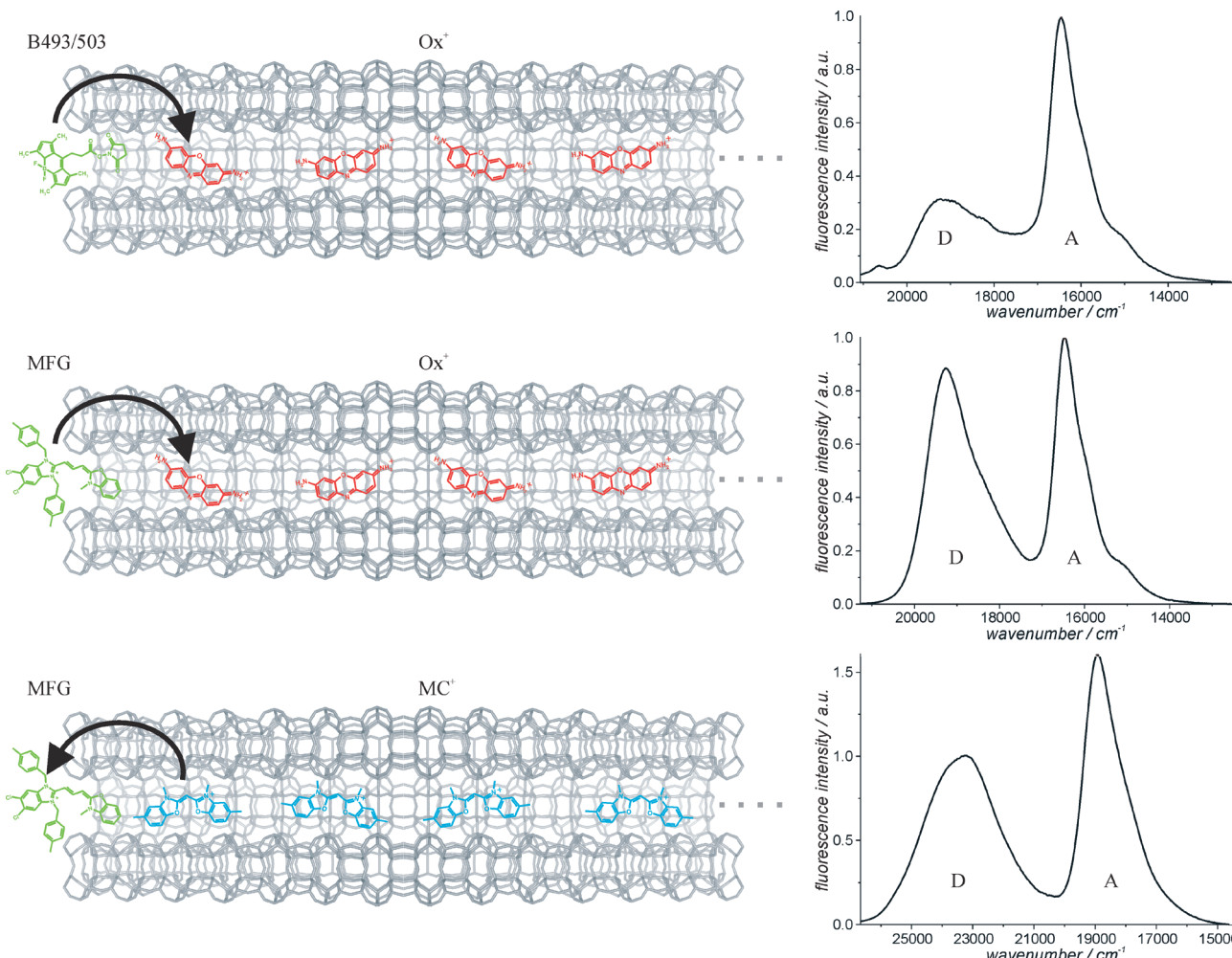


Figure 4. Electronic excitation energy transfer from donor stopcocks to acceptors inside the zeolite channels, and from donors inside to acceptor stopcocks. The emission coming from the donors is denoted with D and that of the acceptors with A. Left: Scheme of three stopcock-plugged antenna systems, top, middle) with donor stopcocks that inject their excitation energy into the channels, bottom) with an acceptor stopcock that traps the excitation energy from inside the channel. Right: corresponding emission spectra after selective excitation of the donor. The donors were selectively excited at $21\,740\,\text{cm}^{-1}$ (top), $22\,000\,\text{cm}^{-1}$ (middle), and $28\,570\,\text{cm}^{-1}$ (bottom).

Ox^+ -zeolite crystals modified with one B493/503 molecule per channel after exciting the B493/503. The Ox^+ loading was chosen to be low, so that 3.5 times more donor molecules were present than acceptor molecules.^[28] Another reversible stopcock, the green fluorescing MitoFluor Green (MFG), is presented in Figure 4, middle, left. Its emission spectrum overlaps with the excitation spectrum of Ox^+ , and, therefore, energy transfer from the stopcock to the Ox^+ molecules inside the channels is expected. The emission spectrum of MFG-modified Ox^+ -zeolite L after selectively exciting MFG is shown in Figure 4, middle, right. The crystals are 30 nm long, the average loading of Ox^+ was again low, and every channel was modified with an MFG molecule on both sides.^[29] The MFG stopcock is attractive, since it can also be used as an energy trap for blue-light-emitting donor dyes, such as MC^+ , inside the channels, see Figure 4, bottom, left. After selectively exciting the MC^+ of MFG modified MC^+ -zeolite L crystals, the emission spectrum of Figure 4, bottom, right, was obtained. The crystal length is also 30 nm; every channel contains approximately two MC^+ molecules in the middle and one MFG stopcock at every channel entrance.^[28]

Covalently bound stopcocks form a bonding via $-\text{Si}-\text{O}-\text{Si}-$ and $-\text{Si}-\text{O}-\text{Al}-$ where we distinguish between: i) covalently bound stopcocks that react via $-\text{Si}(\text{OR})_3$ (where R is an alkyl group) and that cannot enter the channels;^[26] ii) reaction of the stopcock in the channel;^[30] and iii) sequential functionalization, a very flexible principle.^[31] Electrostatically bound stopcocks contain either a positively charged head or a positively charged tail, where the tail can bear one or more positive charges.^[32,29]

3. Results

3.1. Förster-Type Energy Transfer along a Specified Axis

Förster-type energy transfer along a specified axis, sometimes also denoted as quasi-one-dimensional energy transfer, has been discussed in a number of studies.^[33] Here, we elaborate on *antenna materials* and *stopcock-plugged antenna materials* to study the behavior of the electronic excitation energy transfer within one zeolite crystal. The energy-transfer process in the systems under investigation is of the Förster-type mechanism, and its rate constant k_{EnT} can be expressed by Equation 1

$$k_{\text{EnT}} \propto \frac{\varphi}{\tau} J \frac{\kappa^2}{R^6} \quad (1)$$

where φ and τ are the fluorescence quantum yield and the fluorescence lifetime of the donor, respectively, J is the spectral overlap integral between the donor emission and the acceptor absorption spectra, κ describes the relative orientation of the electronic transition moments, and R is the donor–acceptor distance.

The distance R has a strong effect on the energy-transfer rate constant for the donor–acceptor energy transfer and the donor–donor energy migration. As shown in the visual demon-

stration of the random mixing of donors and acceptors, see Figure 2, mixed dye material, bottom, this distance can be tuned by varying the concentration of dye molecules to change the dye–dye distance. Another elegant way to study the distance dependence of the excitation energy transfer is to introduce a spacer molecule between the donors and the acceptors to separate them locally, as illustrated in Figure 5. To realize this, a definite number of acceptor molecules was first incorporated in the channels of zeolite L. In a second, consecutive step, dif-

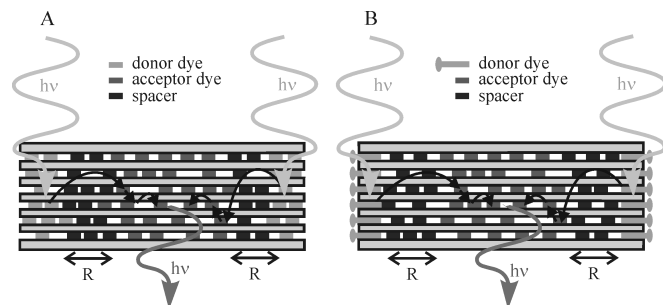


Figure 5. Scheme of zeolite L crystals with acceptor dyes in the middle, followed by different numbers of spacer molecules forming spacer layers of different average thickness, and finally donor dyes at the channel ends. In (B), the donor dye is a stopcock molecule. In (A), the phase boundaries donor–spacer and spacer–acceptor are both diffuse. In (B), all the donors are fixed at the same position, and only the phase boundary spacer–acceptor is diffuse [34].

ferent numbers of spacer molecules were incorporated in the channels already containing the acceptors, forming spacer layers of different thickness; and, in a third step, equal amounts of donor dyes were added. By selectively exciting the donor, the behavior of the excitation energy (dependent on the number of spacer molecules and therefore on the distance R) could be observed.

With the dye molecules shown in Figure 6, we investigated three systems. Two were synthesized according to Figure 5A, where Py^+ acts as the donor and Ox^+ as the acceptor. The third system was synthesized according to Figure 5B, where BR6G-APTS acts as stopcock donor, and $\text{Ox}1^+$ as acceptor.

Specific attachment of the triethoxy group of this donor stopcock at the entrance of the channels was made possible by the findings reported by Calzaferri and co-workers.^[26] The spacer molecules—in our case dyes as well—must be chosen so that they do not participate in the energy-transfer process, that is, they should not absorb where the donor is excited and they should not trap the energy from the donor. In the first and the third systems, DMPOPOP was used as the spacer molecule, forming the $\text{Py}^+, \text{DMPOPOP}, \text{Ox}^+$ -zeolite L (I) and the BR6G-APTS,DMPOPOP,Ox1⁺-zeolite L (III) antenna system, whereas in the second system, MC^+ was used to form the $\text{Py}^+, \text{MC}^+, \text{Ox}^+$ -zeolite L (II) antenna system. For (I) and (II), 840 nm long zeolite L crystals were used; whereas, for (III), the crystals were 300 nm long. The left column of Figure 7 shows the excitation and emission spectra of the individual dye molecules inserted into zeolite L.

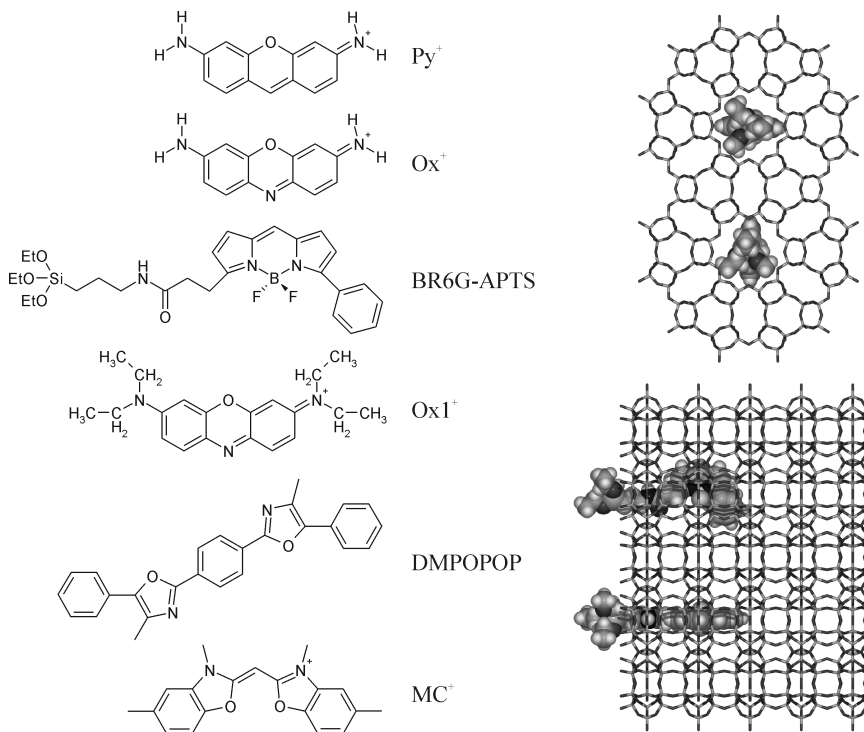


Figure 6. Left: Dyes used for the loading of zeolite L; Py^+ and BR6G-APTS (donors), Ox^+ and Ox^{1+} (acceptors), DMPOPOP and MC^+ (spacers). Right: Framework of two zeolite channels plugged on one side with BR6G-APTS. Top: view along the c axis, bottom: side view perpendicular to the c axis.

For the three systems, a series of four different samples was synthesized. The amount of donor and acceptor was kept constant, whereas the amount of spacer—DMPOPOP or MC^+ —was increased from sample 1 to sample 4, in all series. From the amount of spacer, the average number of spacer molecules n per spacer layer can be calculated, to characterize the averaged length of the spacer layer given as distance R . Emission spectra of the different samples were recorded. Therefore, the donor was selectively excited and the spectra were scaled to the same height as the donor emission (see Figure 7, right column). In all three systems, the first sample with the smallest spacer layer shows the highest acceptor fluorescence intensity. With an increasing amount of spacer molecules per layer, less and less energy transfer occurs and, therefore, the acceptor fluorescence intensity decreases. The distance dependence of the probability P for Förster-type long-range energy transfer from an electronically excited donor to an acceptor can, in a simplified manner, be expressed by Equation 2

$$P = \frac{1}{1 + \left(\frac{R}{R_0}\right)^a} \quad (2)$$

where R_0 is the Förster radius. The exponent a is equal to six^[35] for three-dimensional systems, equal to four^[36] for two-dimensional systems, and becomes equal to two^[37] in one-dimen-

sional systems. We have plotted the acceptor fluorescence intensity versus $1/(1+n^a)$ for different values of a , ranging from 6 to 1, and we found that all data obey an $a=2$ dependence. We illustrate this in Figure 8. The intensity, I_{rel} , does not go to zero as $(1+n^2)^{-1} \rightarrow 0$. This is due to the fact that the absorbtivity of the acceptor is small, but not zero, at the wavelength of excitation.

By multiplying the number of spacer molecules by their lengths, the apparent distance R is obtained; see Table 1. The length of DMPOPOP is 2.02 nm, that of MC^+ 1.48 nm.

The spectral overlap integrals and the corresponding Förster radii in parentheses, calculated for a numerically estimated κ_{DA}^2 value of about one and an estimated refractive index of 1.4, are $J_{\text{Py}^+, \text{Ox}^+} = 2.3 \times 10^{-10} \text{ cm}^6 \text{ mol}^{-1}$ (6.1 nm) and $J_{\text{BR6G-APTS}, \text{Ox}^{1+}} = 5.6 \times 10^{-10} \text{ cm}^6 \text{ mol}^{-1}$ (7.1 nm). In (I) and (II), the values of R range from 17 nm up to 50 nm, which is far too high, all the more considering that there is empty space between the spacer molecules. In both systems, the donors are dyes that also enter the channels. The dyes cannot glide past each other within one

channel, but their position can overlap with the neighboring channels. This reveals a staggered profile of the phase boundaries. As a consequence, some donor–acceptor pairs lay closer together than anticipated by the values of R . Replacing the donors by stopcock molecules results in a less-diffuse phase boundary. This is the case in (III). Here, all the stopcock donors are fixed at the same position, and only one staggered phase boundary from the spacer to the acceptor is left. The values for R in (III) are too large, but they are closer to the range that reflects the donor–acceptor distance. We will discuss in Section 3.3 how these values can be understood.

Time-resolved data for the luminescence decay of the donor for (I) and (II), of the same samples, are reported in Table 2. The data was evaluated with a two-exponential fit with lifetimes τ_1 and τ_2 , the factor f_1 indicating the fraction of photons that decay with lifetime τ_1 . A Py^+ –zeolite L sample with a corresponding loading decays with a mean lifetime $\langle \tau \rangle = 2.4 \text{ ns}$.^[38] The decay of the donor in sample 4 of (I) is much faster, owing to the energy transfer, and it gets faster and faster from samples 4 to 1. This is in agreement with the steady-state emission spectra of these samples. The luminescence decay of the donor of (II) is already very fast for sample 4, and then becomes faster still for samples 4 to 1. This is due to greater energy transfer in sample 4, which can be seen in the steady-state spectra in Figure 7, middle, which show that the acceptor fluorescence intensities are higher than in the samples of (I).

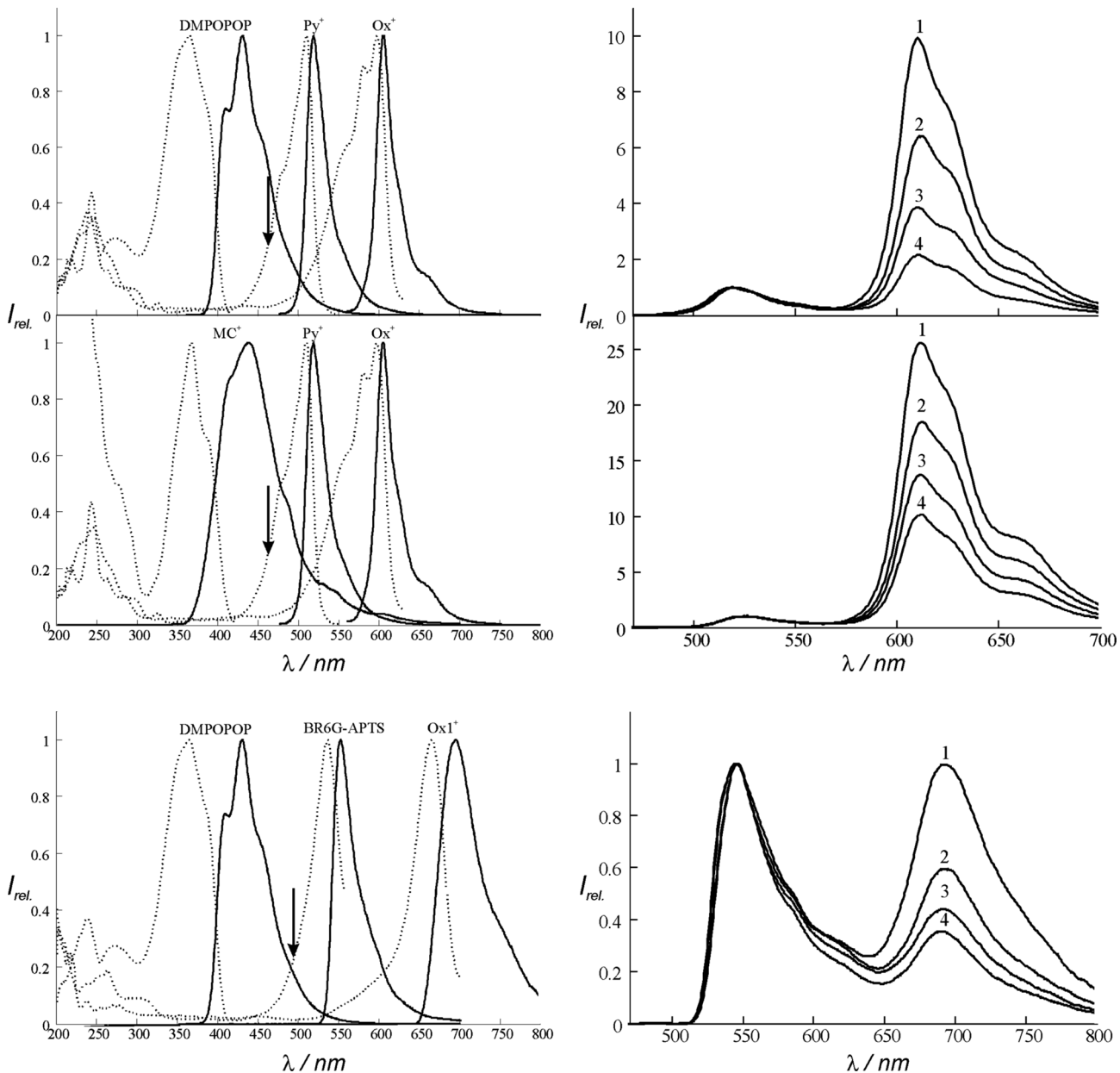


Figure 7. Left: Excitation (dot) and emission (solid) spectra of the applied dye molecules. Right: Fluorescence spectra (scaled to the maximum of the donor emission) for (I) (top), (II) (middle), and (III) (bottom), with different amounts of spacer, after selective excitation of the donor indicated by the arrows on the left. The number of spacer molecules n per layer is given in parentheses: Top: 1 (8.5), 2 (11), 3 (16), 4 (22.5). Middle: 1 (15), 2 (17.5), 3 (24), 4 (36.5). Bottom: 1 (2.67), 2 (4), 3 (6), 4 (10). The inserted amount of donor and acceptor was kept constant in all three systems.

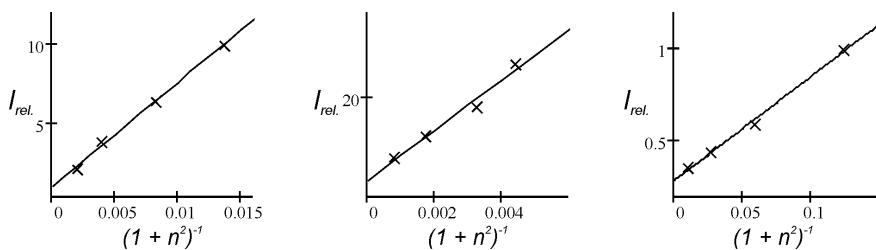


Figure 8. Intensities $I_{rel.}$ of the acceptor fluorescence versus $(1 + n^2)^{-1}$, which is the averaged number of spacer molecules n per spacer layer: left: (I); middle: (II); right: (III).

Table 1. Average number of spacer molecules n per layer for every sample of the three systems, with the apparent mean distances R .

Sample	n spacer	(I)		(II)		(III)	
		R [nm]	n spacer	R [nm]	n spacer	R [nm]	n spacer
1	8.5	17	15	22	2.7	5	
2	11	22	17.5	26	4	8	
3	16	32	24	35	6	12	
4	22.5	46	36.5	53	10	20	

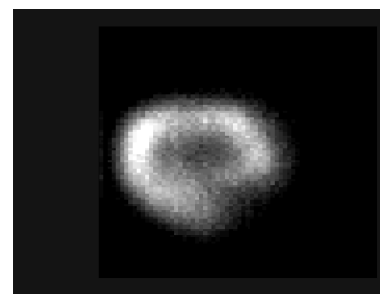
Table 2. Luminescence decay, in nanoseconds, of the donor Py⁺ of the samples of (I) and (II), excited at 465 nm and observed at 520 nm.

System	Sample	$\langle \tau \rangle$	τ_1	τ_2	f_1
Py ⁺ -zeolite L		2.4			
(I)	1	0.13	0.007	1.26	0.90
	2	0.27	0.105	2.00	0.91
	3	0.45	0.11	1.43	0.75
	4	0.89	0.24	2.16	0.66
(II)	1	0.21	0.05	2.96	0.95
	2	0.22	0.04	3.07	0.94
	3	0.25	0.04	2.47	0.91
	4	0.29	0.04	2.75	0.91

3.2. Time-Resolved Measurements on Single Crystals

Time-resolved fluorescence images were recorded at the wavelength of the donor emission band and the acceptor emission band. The position and the fluorescence decay in the dye-loaded zeolite crystals can be correlated in the measurements we have carried out. The fluorescence intensity images of BR6G-APTS-zeolite L crystals containing only stopcock molecules at the channel entrances confirm the localization of the stopcock at the base of the zeolite, where the fluorescence is strongest. This is best seen at the beginning of the measurement and becomes more and more blurred with increasing data-collection time, owing to decreasing contrast. The image in Figure 9 was taken at a time when the original fluorescence intensity distribution could still partially be seen.

We first studied the fluorescence decay of the same crystals as shown in Figure 9 modified only with stopcocks. The result of such a measurement is shown in Figure 10. The sample was excited at 495 nm. The diagram reveals that the decay can be well described by means of a single exponential. We found that the time-resolved measurements of all crystals we investigated—those only modified with stopcocks, and those also containing Ox1⁺ plus spacer and stopcocks, which we refer to as sample (III)—show very good reproducibility from crystal to crystal. Thus, the

**Figure 9.** Fluorescence intensity image of an 840 nm long BR6G-APTS-zeolite L crystal in dichlorobenzene, showing the spatial distribution of the fluorescence.

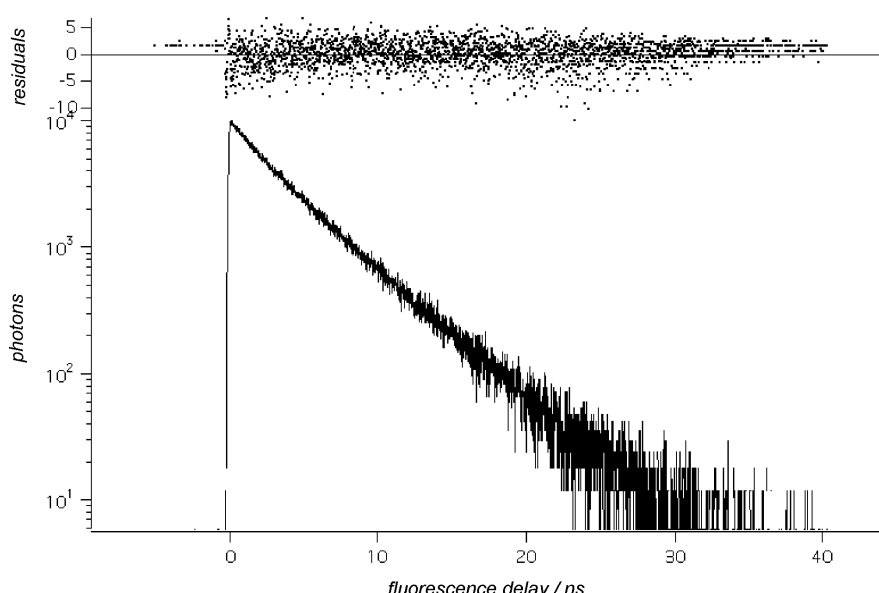
multiexponential decay we observed in (III) does not reflect a heterogeneity of the sample and is indeed due to the presence of the energy transfer in the zeolites. We also found that the exact decay shape in (III) is more complex than a simple biexponential and, thus, better described by fractional power of time, and that the fluorescence of the acceptor molecule was delayed with respect to that of the donor.

3.3. Theoretical Reasoning

In order to better understand the system, some theoretical reasoning is reported.

3.3.1. Phase Boundaries

By incorporating different dyes consecutively in the channels of zeolite L, the crystal is divided into compartments where the density of one dye is dominant, since the conditions are

**Figure 10.** Average fluorescence decay of ten BR6G-APTS-zeolite L crystals. The normalized difference between decays and the average has no time structure.

such that the dyes cannot glide past each other. However, the phase boundaries are relatively diffuse. We describe the distribution of the dye molecules on the phase boundaries of the different compartments within the zeolite crystal by assuming that we have a uniform, random distribution of the dye molecules in the channels of zeolite L. This can be modeled by means of a Monte Carlo calculation, similar to the approach of Yatskou et al.^[38] The channels of a zeolite L crystal are divided into sites that can be either empty or occupied by a dye molecule, see Figure 11, top. We take a zeolite L crystal with 1000 channels, each channel containing 300 sites, and fill all of them randomly with an average of 90 dye molecules. The resulting occupation probability p for this dye-loaded zeolite L compound is then 0.3. If we plot the distribution h_p versus p for these 1000 channels and normalize the incidences to 1 (y axis), see Figure 11, left, it shows that a Gaussian distribution results, with a mean loading of $p=0.3$. Figure 11, right, depicts h_S versus the number of empty sites S between two occupied sites for the same zeolite L crystal, scaled to one. $S=0$ means that there is no empty site between two dye molecules; at $S=1$, there is one empty site between two dyes, etc.

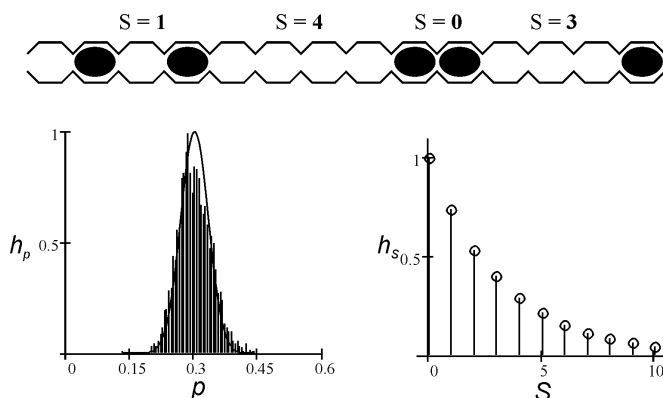


Figure 11. Top: Scheme of a zeolite channel with sites that can be either empty or filled with a dye molecule (dark ovals). S indicates the number of empty sites between two dye molecules. Left: Diagram of the Gaussian distribution (solid) of dye-loaded zeolite channels with a mean occupation probability (p) of 0.3. The bars represent the number of channels having a certain p , normalized to one. Right: Distribution h_S versus S between two occupied sites when the occupation is 0.3, scaled to one.

We now look at a crystal with 40 parallel channels, each channel having 60 sites. We then randomly distribute one kind of dye molecule among these sites, with $p=0.3$. A schematic image of such a zeolite crystal is shown in Figure 12, top. The dye molecules are represented as dark dots. In a consecutive step, we add another type of dye molecule. Therefore, we virtually seal the channels at the right side of the crystal and fill the channels only from the left side. This is a simplification we can apply without loss of information. In the experiment, we have only the first dyes that are pushed further into the centre of the crystal and the second dyes entering at both crystal endings. Here, we fill the same amount of a second type of dye molecules from the left side. This case is shown Figure 12, bot-

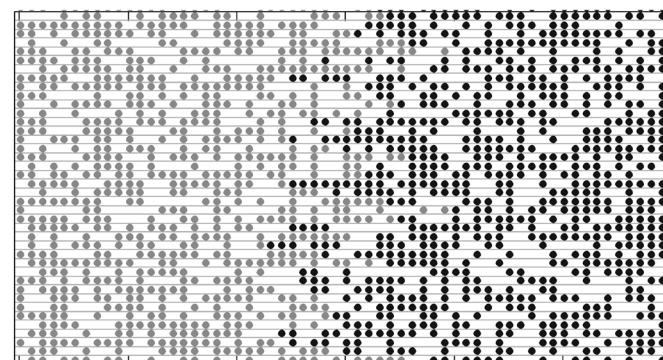
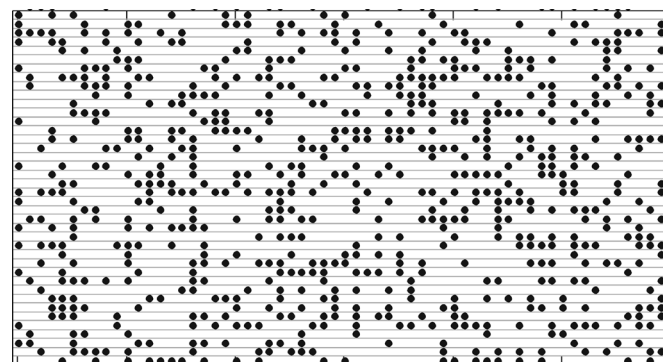


Figure 12. Simulated images of two zeolite L crystals, each contains 40 parallel channels, each channel contains 60 sites. Top: The sites are randomly filled with dye molecules (dark dots); $p=0.3$. Bottom: The sites are first randomly filled with dye molecules (dark dots), while after virtually sealing the right channel entrances, another type of dye (light dots) was consecutively filled in the channels from the left side. For both dyes, $p=0.3$, so that overall $p=0.6$. The phase boundaries extend over 10 to 12 sites.

tom, where the second type of dye molecule is represented as light dots. We notice the increase in the dye content. The overall occupation probability increases to 0.6. A close look at the phase boundary reveals the staggered profile of the borders. The swapping area for this dye concentration extends for 10 to 12 sites. If we consider one site to include two unit cells, this spans an area of 12 to 18 nm.

3.3.2. Energy Migration and Trapping

Excited-state dynamics of energy-transferring systems are often simulated using lattice models.^[39,40] It has been reported by Gfeller and Calzaferri^[41] that the Förster energy migration and transfer occurring in a zeolite L crystal, containing dye molecules and traps, can be described as a random walk in which the energy-transfer steps are incoherent and occur from averaged initial states. The dyes have an electronic-transition dipole moment $\mu_{S_i \leftarrow S_0}$. The distribution can be described on a double cone with a half-cone angle that can lie between 0° and 90°, with respect to the c axis, depending on size and shape.^[20] The individual energy-transfer steps are calculated based on dipole–dipole interactions. A certain time after the irradiation, the energy-migration process gets more and more diffuse, and

a constant-diffusion coefficient can be defined. We will now use this approach to calculate the energy-transfer efficiency depending on the thickness of the spacer layer of a system as illustrated in Figure 13, with donors in the center, followed by the spacer layers and acceptor stopcocks.

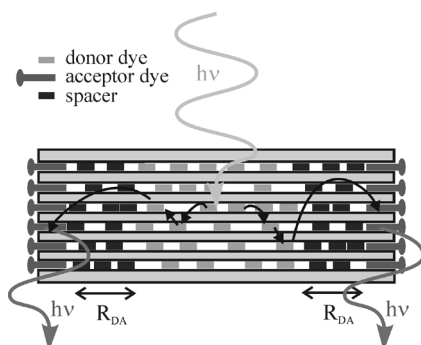


Figure 13. Scheme of a stopcock-plugged antenna material. The donors are located in the center of the crystal, followed by the spacer layers. The traps are stopcock molecules, located at the channel entrances.

The calculation was carried out according to a similar procedure described by Barzykin and Hashimoto.^[40] It describes the system right after exciting the donor, when donor fluorescence and trapping of the excitation energy by the acceptor as a function of R are the only processes to be considered. The luminescence intensity of the donor is proportional to the number of donor molecules that are in an electronically excited state at time t . The same is true for the acceptor. Therefore, we can plot the fluorescence decay of the donors and the acceptors in the absence or presence of each other, see Figure 14.

By setting the donor fluorescence to be one, we can calculate the value for the corresponding acceptor fluorescence for systems with increasing number of spacer molecules. This shows the same $\alpha=2$ dependence as in the experiments, see Figure 15.

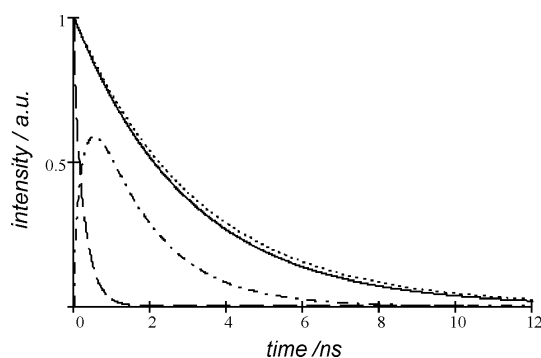


Figure 14. Comparison of the fluorescence decay of the donor (dot) and the acceptor (solid) in the absence of each other, and the donor (dash-dot) and the acceptor (dashed) in the presence of each other. The decay of the donor and acceptor in the absence of each other nearly coincides because they have almost the same natural lifetime τ . The faster decay of the donor in the presence of the acceptor indicates energy transfer, and in the fluorescence of the acceptor in the presence of the selectively excited donor, a rise with a maximum at about 0.5 ns can be seen.

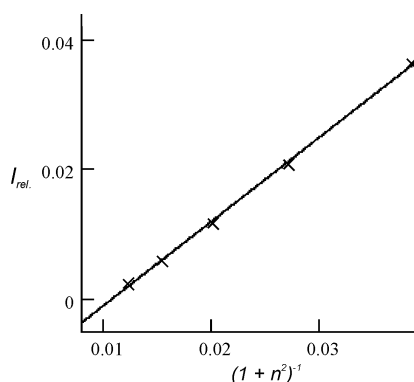


Figure 15. Calculated plot of $I_{\text{rel.}}$ of the acceptor fluorescence versus $(1 + n^2)^{-1}$: It shows an $\alpha=2$ dependence results for a calculated system where the energy migration and transfer steps are described as a random walk by means of Markov chains.

4. Conclusions

We have shown that the basic concept of filling luminescent dyes into hexagonal crystals, which consist of one-dimensional channels with molecular diameters and tuneable lengths, leads to new inorganic–organic host–guest materials with fascinating properties and many options for chemical modification. The concepts described are not limited to zeolite L as a host, but an attractive feature of this zeolite is that neutral as well as cationic dyes can be inserted, and that methods for tuning size and morphology of chemically pure crystals are known. For many dyes, insufficient space is available in the zeolite channels for electronic overlap, so that the monomer properties of the dyes are maintained. This allows light harvesting within a certain volume of a dye-loaded nanocrystalline zeolite, and transport without radiation to both ends of the cylinder, or from the ends to the center. By attaching an acceptor or donor stopcock fluorophore at the ends of the zeolite L channels, which can trap or inject electronic excitation energy from or to the crystal, coupling to an external device is made possible. This offers fascinating possibilities for exploring excitation-energy-transfer phenomena and opportunities for developing new photonic devices.

The experimental data reported in Figures 7,8, and in Tables 1,2 can only be understood in terms of Förster long-range energy transfer. The trivial mechanism would not cause a shortening of the donor luminescence lifetime and there would be no (or a much weaker) distance dependence. The change in distance is more than one order of magnitude smaller than the wavelength of the light. We found that varying the number of spacer molecules n per layer has a strong effect on the energy-transfer rate, as can be seen in the fluorescence intensities of the acceptors in samples where the number of spacer molecules is different. This can be seen in the time-resolved measurements, too, where the mean lifetimes $\langle \tau \rangle$ of the donor increase with increasing number of spacer molecules, owing to less energy transfer to the acceptor. (II) has a much shorter $\langle \tau \rangle$ than (I), although n for (II) is higher in all samples. From this, we as-

sume that MC^+ is more packed than DMPOPOP. The time-resolved measurements on single crystals show the spatial distribution of the fluorescence at the base of the zeolite crystal and the monoexponential fluorescence decay of the BR6G-APTS-zeolite L. Thus, the more complex behavior of (III) can only be explained by assuming energy transfer from the stopcock to Ox^{1+} . The meaning of the averaged values of R has been discussed. As a consequence, some donor–acceptor pairs lay closer together than anticipated by these values. The phase boundaries were studied by modeling the distribution of dye molecules and empty sites within a zeolite crystal with a Monte Carlo simulation. This also shows that the swapping area between the two phase boundaries is relatively large. Replacing the donors by stopcock molecules results in a much less diffuse phase boundary. Then, all stopcock donors were fixed in the same position, and only one staggered phase boundary from the spacer to the acceptor was left. This is the case in (III). The correlation of the acceptor fluorescence intensity versus n leads to a linearization at $1/(1+n^2)$. Of course, the individual transfer step can occur in another direction, for example, to a neighboring channel, but this proportionality suggests that, by summing up the individual steps, the statistical mean of the energy transfer in the dye-loaded zeolite L crystals is directed quasi-one-dimensionally along the c axis of the cylinder. By describing such dye-loaded zeolite L crystals theoretically as a random walk by means of Markov chains, analogous to the procedure described by Gfeller and Calzaferri,^[41] the same $1/(1+n^2)$ dependence was observed. The reported results substantially enhance the knowledge of the energy-transfer and migration processes occurring in dye-loaded zeolite L.

5. Experimental

Chemicals: Zeolite L crystals were synthesized and characterized as described previously [16a]. The potassium exchanged form was used, with an average crystal length of 30 nm for B493/503, Ox^+ -zeolite L, MFG, Ox^+ -zeolite L, and MFG, MC^+ -zeolite L, 840 nm for Py^+ , DMPOPOP, Ox^+ -zeolite L and Py^+ , MC^+ , Ox^+ -zeolite L, and 300 nm for BR6G-APTS, DMPOPOP, Ox^{1+} -zeolite L. Py^+ and Ox^+ were synthesized and purified as reported in the literature [42]. B493/503 (BODIPY 493/503 SE, Molecular Probes), MFG (Molecular Probes), DMPOPOP (Fluka), MC^+ (CIBA-GEIGY AG) and Cryptofix 222 (Fluka) were used as received. BR6G-APTS was made by substituting BODIPY-R6G (BODIPY R6G SE, Molecular Probes) with 3-aminopropyltriethoxy-silane (Fluka). The two compounds were dissolved in Cl_2CH_2 and stirred for 1 h. Then, the Cl_2CH_2 was evaporated, and the precipitate was washed twice with cyclohexane [31].

B493/503, Ox^+ -zeolite L and MFG, Ox^+ -zeolite L: Ox^+ was first incorporated into the channels of zeolite L via ion exchange in water. Therefore, zeolite L was suspended in water and sonicated 20 min to avoid aggregation of the crystals. Then, an aqueous solution of Ox^+ containing the required amount of Ox^+ was added and refluxed 7 h at 100 °C. The Ox^+ -loaded zeolite L crystals were washed with methanol to remove the Ox^+ quantitatively from the surface. B493/503 and MFG were adsorbed from cyclohexane onto the zeolite L crystals. The Ox^+ -loaded zeolite L crystals were dissolved in cyclohexane and sonicated for 20 min. Then, an appropriate amount of stopcock, dissolved in cyclohexane, was added, and the mixture was sonicated for another 30 min. After separating the supernatant by centrifugation, B493/503, Ox^+ -zeolite L and MFG, Ox^+ -zeolite L were obtained.

MFG, MC^+ -zeolite L: Zeolite L was suspended in a mixture of *n*-butanol/water (1:10) and sonicated for 20 min. A solution of MC^+ in the same *n*-butanol/water mixture was added to the zeolite L suspension, containing also an excess Cryptofix 222 [42]. By refluxing it for ≥48 h at 65 °C, the insertion rate was about 40 to 50 % of the preset amount of MC^+ . The MC^+ -zeolite L crystals were then washed with methanol. MFG was attached as described for MFG, Ox^+ -zeolite L.

Py^+ , DMPOPOP, Ox^+ -zeolite L: The neutral DMPOPOP was inserted from the gas phase [8]. Therefore, Ox^+ -loaded zeolite L crystals were transferred in a glass ampoule and dehydrated under vacuum (3×10^{-2} mbar; 1 bar = 10^5 Pa) at 80 °C for 24 h to empty the adsorption sites in the channels. Then, the required amount of DMPOPOP was added, and the ampoule was sealed. The incorporation took place by heating in a rotating furnace at 150 °C for six days. Afterwards, the DMPOPOP, Ox^+ -zeolite L crystals were washed with *n*-butanol and rehydrated in an exsiccator containing a saturated solution of potassium acetate. In the end, Py^+ was again incorporated in water. DMPOPOP, Ox^+ -zeolite L was suspended in water, and an aqueous solution of Py^+ containing the required amount of Py^+ was added, and it was refluxed for 30 min at 100 °C. Py^+ , DMPOPOP, Ox^+ -zeolite L was washed again with methanol to get rid of all dye molecules on the crystal surface.

Py^+ , MC^+ , Ox^+ -zeolite L: The incorporation of MC^+ in the channels of Ox^+ -zeolite L was carried out stepwise to achieve higher loadings. The MC^+ , Ox^+ -zeolite L crystals were then washed with methanol, and the insertion was repeated up to four times. In the end, Py^+ was added according to the procedure described for Py^+ , DMPOPOP, Ox^+ -zeolite L.

BR6G-APTS, DMPOPOP, Ox^{1+} -zeolite L: Zeolite L was suspended in toluene and sonicated for 20 min. Then, a solution of Ox^{1+} in toluene, containing the required amount of Ox^{1+} and an excess of Cryptofix 222, was added and heated for 7 h at 65 °C. The Ox^{1+} -loaded zeolite L crystals were washed with methanol. The neutral DMPOPOP was then inserted from the gas phase, according to the procedure for Py^+ , DMPOPOP, Ox^+ -zeolite L. In the end, BR6G-APTS was added by dissolving DMPOPOP, Ox^{1+} -zeolite L in Cl_2CH_2 and adding the required amount of stopcock. The mixture was sonicated for 30 min and stirred 20 h at room temperature [26]. Then, BR6G-APTS, DMPOPOP, Ox^{1+} -zeolite L was dried, dissolved in *n*-hexane and refluxed for 2 h, and again washed with methanol.

Thin-Layer Preparation: 100 μL of dye-loaded zeolite L suspended in *n*-butanol (~1 mg in 300 μL) was dropped on a quartz plate (\varnothing 1.6 cm) and the solvent was evaporated in air. The quartz plate was therefore covered with a Petri dish.

Emission and excitation spectra were recorded on a Perkin–Elmer LS 50B luminescence photospectrometer with appropriate cut-off filters. The samples were measured as thin layers on quartz. Absorption spectra were recorded on a Perkin–Elmer Lambda 900 UV-Vis–near-IR spectrophotometer. Time-resolved measurements were carried out as described by Yatskou et al. [38]. The samples were excited at 465 nm, detected at 520 nm, and the slits' width was 4 nm. For the time-resolved measurements on single crystals, the fluorescence lifetime images of the zeolites were obtained by using a fluorescence decay microscope setup composed of a picosecond Ti-Sa laser with doubling and pulse picking (excitation 495 nm, 4 MHz) (Tsunami, Spectra Physics), a time- and space-correlated single-photon counting detector (Europhoton GmbH, Germany), and an inverted microscope with a 100 1.44 numerical aperture (NA) oil objective (Nikon). The instrument response time was 250 ps (FWHM) and the spatial resolution of our setup was 300 nm (FWHM) [43].

Optical Fluorescence Microscopy Images: Images were obtained using an Olympus BX 60 device equipped with a Kappa CF 20 DCX Air K2 CCD camera [8].

Amount of Dye: The amount of dye inside the channels was determined by first destroying the zeolite framework with HF: 100 μL of an 8 % solution of HF was added to a solution of 3.9 mL *n*-butanol containing 1 mg of dye-loaded zeolite L in a polypropylene tube and sonicated for 5 min. The amount of dye left in the solution was determined by measuring the UV-vis absorption spectrum.

Received: May 9, 2005

Final version: June 23, 2005

Published online: October 19, 2005

- [1] a) G. Kodis, P. A. Liddell, L. de la Garza, P. Ch. Clausen, J. S. Lindsey, A. L. Moore, T. A. Moore, D. Gust, *J. Phys. Chem. A* **2002**, *106*, 2036. b) R. K. Clayton, *Photosynth. Res.* **2002**, *73*, 63. c) T. Ritz, A. Damyanovic, K. Schulten, *ChemPhysChem* **2002**, *3*, 243. d) W. Lubitz, *Phys. Chem. Chem. Phys.* **2002**, *4*, 5539.
- [2] A. N. Macpherson, P. A. Liddell, D. Kuciauskas, D. Tatman, T. Gillbro, D. Gust, T. A. Moore, A. L. Moore, *J. Phys. Chem. B* **2002**, *106*, 9424.
- [3] M. Ganschow, Ch. Hellriegel, E. Kneuper, M. Wark, C. Thiel, G. Schulz-Ekloff, Ch. Bräuchle, D. Wöhrle, *Adv. Funct. Mater.* **2004**, *14*, 269.
- [4] S. Hashimoto, T. Mutoh, H. Fukumura, H. Masuhara, *J. Chem. Soc., Faraday Trans.* **1996**, *92*, 3653.
- [5] R. Hoppe, G. Schulz-Ekloff, D. Wöhrle, Ch. Kirschhock, H. Fuess, L. Uytterhoeven, R. Schoonheydt, *Adv. Mater.* **1995**, *7*, 61.
- [6] X. Gong, J. C. Ostrowski, D. Moses, G. C. Bazan, A. J. Heeger, *Adv. Funct. Mater.* **2003**, *13*, 439.
- [7] H. Maas, G. Calzaferri, *Angew. Chem. Int. Ed.* **2002**, *41*, 2284.
- [8] G. Calzaferri, S. Huber, H. Maas, C. Minkowski, *Angew. Chem. Int. Ed.* **2003**, *42*, 3732.
- [9] G. Calzaferri, M. Pauchard, H. Maas, S. Huber, A. Khatyr, T. Schaafsmma, *J. Mater. Chem.* **2002**, *1*, 1.
- [10] L. Tosheva, V. P. Valtchev, *Chem. Mater.* **2005**, *17*, 2494.
- [11] A. Dong, N. Ren, W. Yang, Y. Wang, Y. Zhang, D. Wang, J. Hu, Z. Gao, Y. Tang, *Adv. Funct. Mater.* **2003**, *13*, 943.
- [12] Ch. Baerlocher, W. M. Meier, D. H. Olson, *Atlas of Zeolite Framework Types*, 5th ed., Elsevier, Amsterdam **2001**.
- [13] T. Ohsuna, B. Slater, F. Gao, J. Yu, Y. Sakamoto, G. Zhu, O. Terasaki, D. E. W. Vaughan, S. Qiu, C. R. Catlow, *Chem. Eur. J.* **2004**, *10*, 5031.
- [14] O. Larlus, V. P. Valtchev, *Chem. Mater.* **2004**, *16*, 3381.
- [15] D. W. Breck, *Zeolite Molecular Sieves*, John Wiley and Sons, New York **1974**.
- [16] a) S. Megelski, G. Calzaferri, *Adv. Funct. Mater.* **2001**, *11*, 277. b) A. Zabala Ruiz, D. Brühwiler, G. Calzaferri, *Monatsh. Chem.* **2005**, *136*, 77.
- [17] M. Tsapatsis, *AICHE J.* **2002**, *48*, 654.
- [18] S. Hashimoto, M. Hagiri, N. Matsubara, S. Tobita, *Phys. Chem. Chem. Phys.* **2001**, *3*, 5043.
- [19] B.-L. Su, V. Norberg, C. Hansen, *Langmuir* **2000**, *16*, 1132.
- [20] S. Megelski, A. Lieb, M. Pauchard, A. Drechsler, S. Glauß, C. Debus, A. J. Meixner, G. Calzaferri, *J. Phys. Chem. B* **2001**, *105*, 25.
- [21] a) K. Hoffmann, F. Marlow, J. Caro, *Adv. Mater.* **1997**, *9*, 567. b) K. Hoffmann, U. Rensch-Genger, F. Marlow, *Microporous Mesoporous Mater.* **2000**, *41*, 99. c) K. Hoffmann, U. Rensch-Genger, F. Marlow, in *Host-Guest Systems Based on Nanoporous Crystals* (Eds: F. Laeri, F. Schüth, U. Simon, M. Wark), Wiley-VCH, Weinheim, Germany **2003**, p. 501.
- [22] a) H. L. Casal, J. C. Scaiano, *Can. J. Chem.* **1984**, *62*, 628. b) H. L. Casal, J. C. Scaiano, *Can. J. Chem.* **1985**, *63*, 1308. c) J. C. Scaiano, H. García, *Acc. Chem. Res.* **1999**, *32*, 783.
- [23] G. Calzaferri, O. Bossart, D. Brühwiler, S. Huber, C. Leiggeler, M. K. van Veen, A. Zabala Ruiz, *C. R. Chim.* **2005**, in press.
- [24] M. Pfenniger, G. Calzaferri, *ChemPhysChem* **2000**, *4*, 211.
- [25] M. Pauchard, S. Huber, R. Méallet-Renault, H. Maas, R. Pansu, G. Calzaferri, *Angew. Chem. Int. Ed.* **2001**, *40*, 2839.
- [26] a) T. Ban, D. Brühwiler, G. Calzaferri, *J. Phys. Chem. B* **2004**, *108*, 16348. b) D. Brühwiler, G. Calzaferri, *C. R. Chim.* **2005**, *8*, 391.
- [27] A. Khatyr, H. Maas, G. Calzaferri, *J. Org. Chem.* **2002**, *67*, 6705.
- [28] H. Maas, *Ph.D. Thesis*, Universität Bern **2003**.
- [29] H. Maas, G. Calzaferri, *The Spectrum* **2003**, *16*, 18.
- [30] S. Huber, G. Calzaferri, *ChemPhysChem* **2004**, *5*, 239.
- [31] S. Huber, G. Calzaferri, *Angew. Chem. Int. Ed.* **2004**, *43*, 6738.
- [32] O. Bossart, L. De Cola, S. Welter, G. Calzaferri, *Chem. Eur. J.* **2004**, *10*, 5771.
- [33] a) J. Klafter, J. M. Drake, *Molecular Dynamics in Restricted Geometries*, John Wiley and Sons, New York **1989**. b) S. E. Webber, *Chem. Rev.* **1990**, *90*, 1469. c) J. Klafter, A. Blumen, *J. Chem. Phys.* **1984**, *80*, 875. d) P. Levitz, J. M. Drake, *Phys. Rev. Lett.* **1987**, *58*, 686. e) J. P. S. Farinha, J. G. Spiro, M. A. Winnik, *J. Phys. Chem. B* **2001**, *105*, 4879. f) M. Hopmeier, W. Guss, M. Deussen, E. O. Göbel, R. F. Mahrt, *Phys. Rev. Lett.* **1999**, *82*, 4118.
- [34] a) C. Minkowski, G. Calzaferri, *Chimia* **2005**, *59*, 88. b) C. Minkowski, G. Calzaferri, *Angew. Chem. Int. Ed.* **2005**, *44*, 5325.
- [35] Th. Förster, *Fluoreszenz Organischer Verbindungen*, Vandenhoeck and Ruprecht, Göttingen, Germany **1951**.
- [36] a) B. Valeur, *Molecular Fluorescence*, Wiley-VCH, Weinheim, Germany **2001**. b) J. R. Lakowicz, *Principles of Fluorescence Spectroscopy*, 2nd. ed., Kluwer Academic-Plenum Publishers, NY, **1999**. c) X. F. Wang, B. Herman, *Fluorescence Imaging Spectroscopy and Microscopy*, John Wiley and Sons, New York **1996**.
- [37] H. Kuhn, *J. Chem. Phys.* **1970**, *53*, 101.
- [38] M. M. Yatskou, M. Meyer, S. Huber, M. Pfenniger, G. Calzaferri, *ChemPhysChem* **2003**, *4*, 567.
- [39] B. Gobets, L. Valkunas, R. van Grondelle, *Biophys. J.* **2003**, *85*, 3872.
- [40] A. V. Barzykin, S. Hashimoto, *J. Chem. Phys.* **2000**, *113*, 2841.
- [41] N. Gfeller, G. Calzaferri, *J. Phys. Chem. B* **1997**, *101*, 1396.
- [42] H. Maas, A. Khatyr, G. Calzaferri, *Microporous Mesoporous Mater.* **2003**, *65*, 233.
- [43] L. Schouteten, P. Denjean, R. Pansu, *J. Fluoresc.* **1997**, *7*, 155.